THE JOURNAL OF PHYSICAL CHEMISTRY LETTERS
A JOURNAL OF THE AMERICAN CHEMICAL SOCIETY

pubs.acs.org/JPCL

Letter

Molecular Encapsulation from the Liquid Phase and Graphene Nanoribbon Growth in Carbon Nanotubes

Ana Cadena,* Bea Botka,* Áron Pekker, Cla Duri Tschannen, Chiara Lombardo, Lukas Novotny, Andrei N. Khlobystov, and Katalin Kamarás

Cite This: J. Phys. Chem. Lett. 2022, 13, 9752−9758

Read Online

ACCESS | Metrics & More | Article Recommendations | Supporting Information

ABSTRACT: Growing graphene nanoribbons from small organic molecules encapsulated in carbon nanotubes can result in products with uniform width and chirality. We propose a method based on encapsulation of 1,2,4-trichlorobenzene from the liquid phase and subsequent annealing. This procedure results in graphene nanoribbons several tens of nanometers long. The presence of nanoribbons was proven by Raman spectra both on macroscopic samples and on the nanoscale by tip-enhanced Raman scattering and high-resolution transmission electron microscopic images.

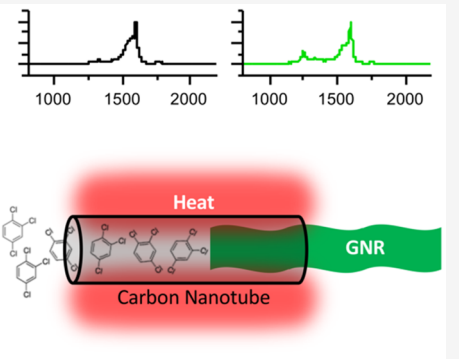

Graphene nanoribbons (GNRs) are one-dimensional objects cut from graphene sheets with important applications in nanoelectronics. Their conformation can be zigzag (ZGNR), armchair (AGNR), or chiral. The ZGNRs are all predicted to be metallic, whereas AGNRs can be metallic or semiconducting, depending on their width. With this variety in size and conformation determining the electronic properties, there arises a need for multiple fabrication methods that are both selective and reproducible.

GNRs can be either produced from graphene by top-down methods or from small molecules by bottom-up procedures.[1] Top-down methods are various forms of lithography or cutting by electron or ion beams or scanning probe tips.[2] Bottom-up procedures have been first performed in solution, for example, branched polyphenylenes converted to highly conjugated graphite structures with high aspect ratio,[3] or two-dimensional (2D) crystals with long carbon chains stabilizing the edges.[4] Oriented chemical reactions on surfaces followed, starting from small planar molecules.[5,6] Another possibility is growing nanoribbons in a confined environment, where, besides the precursor, the container's internal diameter will determine the nanoribbon width. Carbon nanotubes (CNTs) are suitable templates for this purpose, because their diameter matches the size of the most popular nanoribbons 6-AGNR or 7-AGNR. Lim et al.[7] first suggested a two-step mechanism for the formation of inner nanotubes from encapsulated small molecules, where initial mild heat treatment produced GNRs that, on vigorous annealing, formed inner nanotubes through a twisted helical intermediate product. Besides leading to inner tubes of specific chirality, this study also suggested a method for producing encapsulated GNRs by stopping the process after the first step. Although intuition would dictate that fusion reactions of polyaromatic hydrocarbons would all follow this mechanism, this is not a general rule; only some specific reactions proceed through these intermediates, for example, those starting from coronene[8−10] or perylene. Several other starting materials with different structures have been tried since, for example, ferrocene[11,12] as well as precursors containing halogens[13,14] and sulfur.[15,16] These molecules show a surprising variety of structures, including non-six-membered rings and functionalized fullerenes. The full understanding of the mechanism of this self-assembly into GNRs inside nanotubes is an open topic for experimental and theoretical efforts and underlines the need for further synthetic work to extend the selection of materials.

In this work we offer a new, facile method that can be applied to widen this database. We show that graphene nanoribbons with length several tens of nanometers can be grown from 1,2,4-trichlorobenzene (TCB) using a simple procedure. The encapsulation process results in a high filling ratio and does not require subsequent rinsing. We characterized the prepared GNRs, specifically the 6-AGNR, using

Received: June 30, 2022
Accepted: September 28, 2022
Published: October 12, 2022

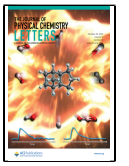

https://doi.org/10.1021/acs.jpclett.2c02046
J. Phys. Chem. Lett. 2022, 13, 9752−9758

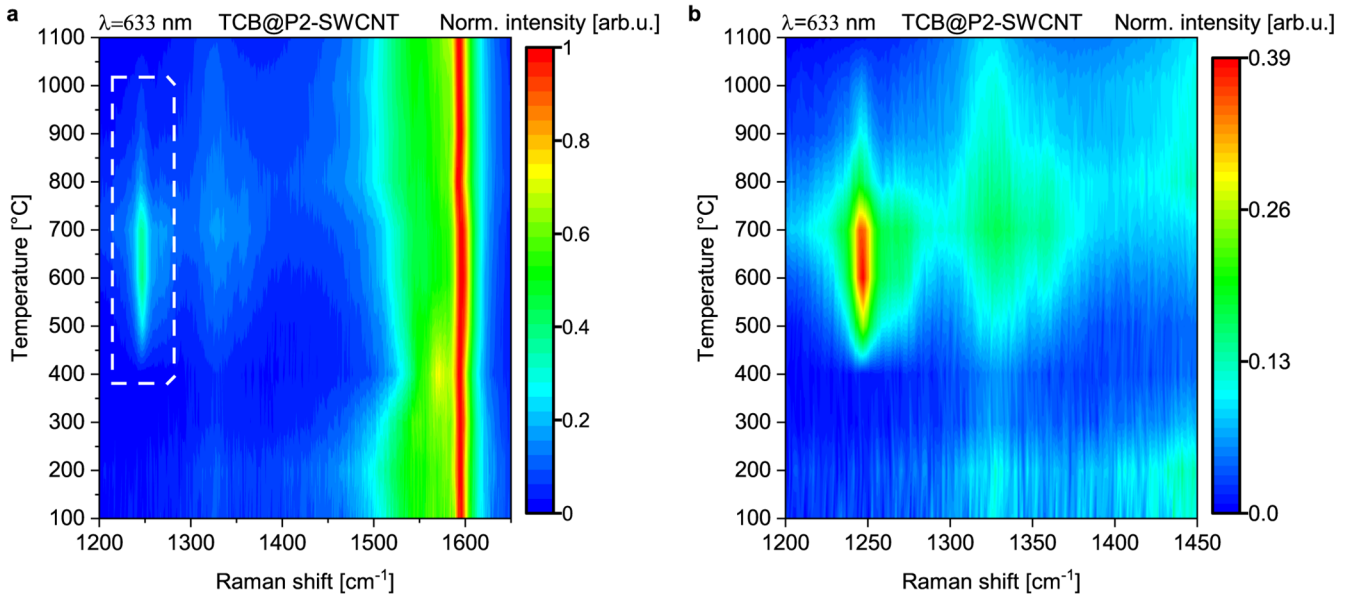

Figure 1. Map representation of the Raman spectra taken during the annealing process. Each spectrum was collected at room temperature after the sample was consecutively annealed at different temperatures (in 100 °C steps) in a tube furnace for 12 h. The sample was kept in vacuum in a closed quartz tube throughout the measurement sequence. The results were combined into a color-coded map indicating GNR formation inside P2-SWCNT in a certain annealing temperature range. (a) TCB@P2-SWCNT annealed from 100 to 1100 °C in 100 °C steps measured with a 633 nm laser through the quartz tube (the spectra were normalized to the SWCNT G mode). (b) Close-up to the nanoribbon's C−H ipb mode (marked by a rectangle) observed in map (a).

Raman spectroscopy, tip-enhanced Raman scattering (TERS), and high-resolution transmission electron microscopy (TEM).

To obtain a nanoribbon with a controlled size and dimension, using CNTs as templates, it is very important to choose an appropriate encapsulation method. Such methods have been reviewed in our previous work.[17] High-temperature procedures can lead to the formation of undesired byproducts.[9] This can be particularly problematic in the case of GNR precursors, as GNR formation is generally initiated inside the nanotube by annealing. However, the molecules may start to react with each other already close to the sublimation temperature, leading to the outer walls of the nanotubes being covered with larger polycyclic aromatic hydrocarbons. Their removal can be problematic, as their solubility is rapidly decreasing with their size. Encapsulation from a solution of the precursor molecules[18] overcomes this problem, as it can be performed at low temperature and is suitable for a broad range of guest molecules. Its major disadvantage stems from the presence of the solvent that can also enter the nanotube channels. This not only leads to lower filling ratios compared to direct encapsulation methods but can also alter the reaction pathway of the precursor inside the cavity.[19] Leaking of the guest molecules can also be problematic during rinsing steps, which are necessary to remove the nonencapsulated precursors. These steps may decrease the filling ratio by diluting the solution in the cavity. An important development was direct immersion in neat organic liquids at room temperature, yielding complete filling of single-walled carbon nanotubes (SWCNTs) that was preserved in aqueous solutions.[20] A comprehensive study of encapsulated systems involving a wide range of nanotube diameters and guest molecules demonstrated the applicability of this method for optical property tuning.[21]

An ideal GNR precursor candidate would thus be a compound that is liquid at room temperature; therefore, it can directly fill the immersed CNTs and be volatile enough so the nonencapsulated molecules can be removed from the outer surface of the nanotubes by evaporation under mild enough conditions before forming ribbons inside. We found that TCB is suitable for this purpose.

Raman spectroscopy is the most widely employed method to detect subtle changes in nanotubes upon physical or chemical interaction with their environment.[22−24] Encapsulation of molecules can be easily detected by observing the shift of the radial breathing mode (RBM), as the molecules inside the nanotube cavity influence the radial expansion and contraction of the nanotube.[25] Data are available for a wide variety of encapsulated molecules.[21,26] In the case of individual nanotubes, a blueshift of the RBM occurs compared to the empty ones. A shift of the RBM can be also detected in bundles of tubes upon filling, though identifying the origin of the shift is more complicated in this case, as the interaction between the nanotubes also alters their RBM. In our work, after exposing the SWCNTs to TCB, a significant blueshift of the RBM mode (around 7 cm^{-1}) was detected with 532, 633, and 785 nm laser excitation (Figure S1, Supporting Information).

Raman spectra of GNRs can also be used for identification. Their most prominent feature is the radial breathing-like mode (RBLM),[27] in the low-frequency part of the spectrum, corresponding to carbon atoms in the two halves of the ribbon moving in-phase in opposite directions. The frequency of this band depends on the ribbon width. As the edges of the ribbons are in most cases terminated by noncarbon atoms, typically hydrogen, C−H vibrations also appear, the most intense among them being the C−H in-plane bending (C−H ipb) mode. The Raman spectra of GNRs are resonant with the exciting laser, the excitation spectrum showing a maximum at their band gap.

Encapsulation of TCB was performed by immersion of single-walled carbon nanotubes (P2, Carbon Solutions, Inc.[28])

https://doi.org/10.1021/acs.jpclett.2c02046
J. Phys. Chem. Lett. 2022, 13, 9752−9758

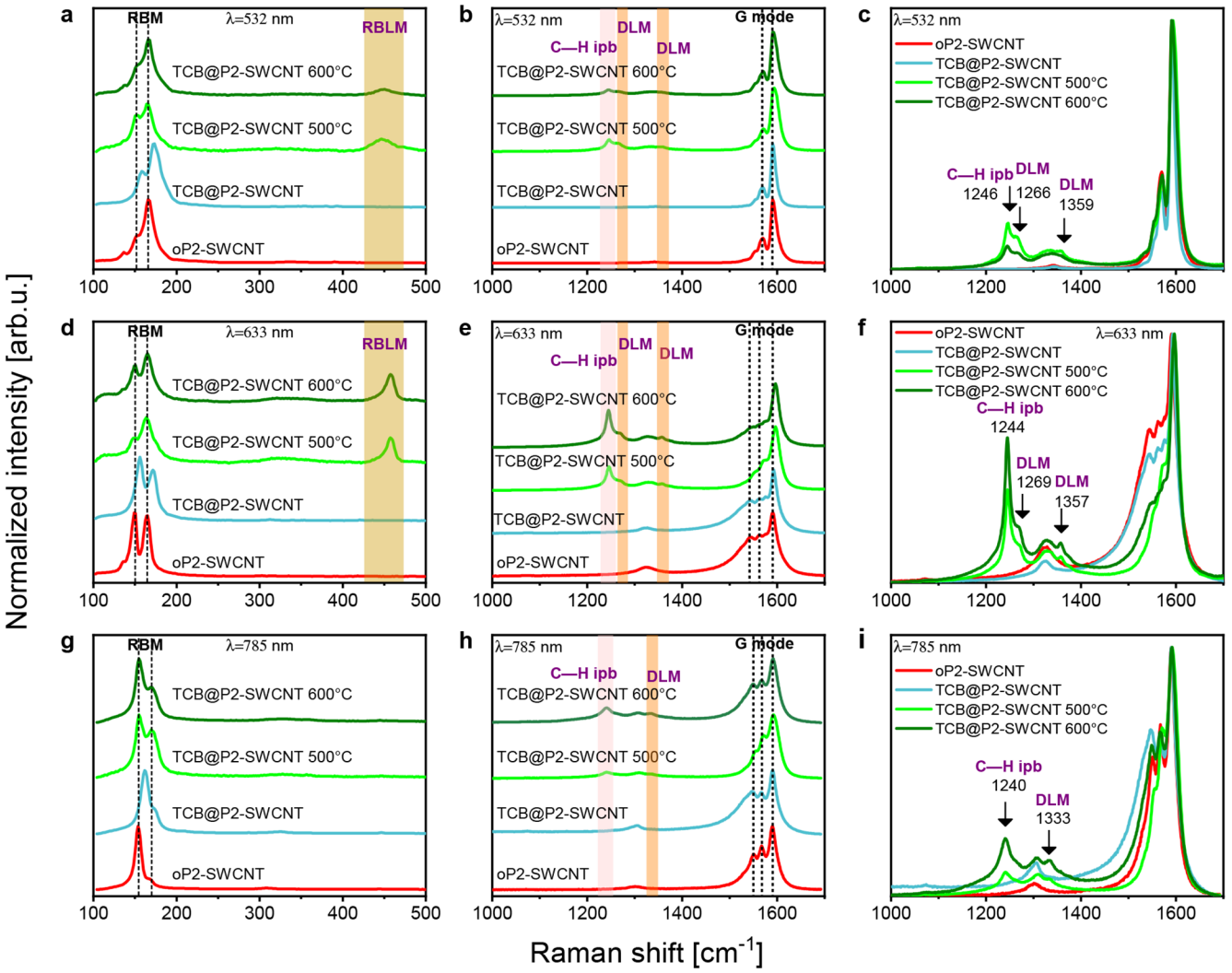

Figure 2. Raman spectra of TCB@P2-SWCNT annealed to 500 and 600 °C compared with opened and filled P2-SWCNT as references. Spectra from the RBLM and C−H ipb-D regions: (a−c) GNR@P2-SWCNT samples measured with 532 nm laser. (d−f) GNR@P2-SWCNT samples measured with 633 nm laser. (g−i) GNR@P2-SWCNT samples measured with 785 nm laser. Low-energy region spectra (a, d, g) are normalized to the RBM and (b, c, e, f, h, i) spectra to the G mode of the SWCNT.

in TCB at room temperature, resulting in the hybrid structure TCB@P2-SWCNT. To identify the ideal temperature at which GNRs form, we used a stepwise annealing protocol and followed the process by Raman spectroscopy. Starting from a cold furnace, the material was first annealed to 100 °C for 12 h and allowed to cool to room temperature, then the Raman spectrum was recorded through the quartz tube; the procedure was repeated in 100 °C steps up to 1100 °C (Figure 1). At this point the quartz tube was opened, and the material was measured under direct illumination, to identify double-walled carbon nanotubes whose RBM bands may be otherwise obscured by the quartz. Finally, the same sample was enclosed again in a quartz tube and annealed to 1200 °C. The recorded Raman spectra are shown in Figure S2, Supporting Information. Based on the excitation profiles reported by Kuzmany et al.,[11] a 633 nm laser can induce a resonant Raman process in 6-AGNRs. We used the C−H ipb mode to track the GNR formation during the annealing process (Figure 1, Figure S2, Supporting Information). Formation of GNRs was first detected after annealing to 500 °C (TCB@P2-SWCNT 500 °C), with the most intense ribbon peaks appearing at 600 °C formation temperature (TCB@P2-SWCNT 600 °C). For formation temperatures above 700 °C the ribbon modes start to diminish, and they completely disappear at the 1100 °C annealing step, while new peaks appear in the RBM region indicating the presence of inner nanotubes (Figure S2, Supporting Information). The conversion into inner tubes indirectly confirms that the detected ribbons were formed in the nanotube interior.

It is useful to put our results in context with the literature. 6-AGNRs were observed to form from ferrocene at similar temperatures as from TCB. In the case of perylene, perylene-3,4,9,10-tetracarboxylic dianhydride, and coronene, ribbon fragments started forming between 500 and 550 °C, and GNRs appeared upon further annealing between 600 and 900 °C.[7−9] 7-AGNRs from 10,10′-dibromo-9,9′-bianthryl were detected already after being annealed at 300 °C.[14]

To perform a thorough characterization, the TCB@P2-SWCNT samples were directly annealed to the temperatures where the signal from the C−H ipb peak was the largest (500−600 °C). To prevent the encapsulated material from leaving the tubes during the low-temperature annealing, the furnace

https://doi.org/10.1021/acs.jpclett.2c02046
J. Phys. Chem. Lett. 2022, 13, 9752−9758

was preheated to 500 °C, then the sample was inserted and kept at this temperature for 12 h. When the cooling step started, one end of the quartz tube was pulled out of the furnace to collect the molecules, if any, leaving the nanotube. The TCB@P2-SWCNT 600 °C sample was prepared starting from the 500 °C sample following the same procedure. Inner tubes were formed by annealing the sample containing the ribbons (TCB@P2-SWCNT 600 °C) to 1200 °C (Figure S3, Supporting Information). Raman spectra were taken using 532, 633, and 785 nm excitation. Both the stepwise and the directly annealed samples were prepared from the same TCB@P2-SWCNT batch; judging the GNR yield by comparing the relative ratio of the ribbon peaks versus the CNT peaks, the directly annealed material shows higher conversion than the stepwise annealed one. The significant blueshift of the RBM observed on the TCB@P2-SWCNT is not present anymore after annealing (Figure 2), indicating a relaxation of the tube walls from the strain exerted by the encapsulated TCB molecules. The latter may show a liquid-like association inside the tubes, similar to water filling,[26] and convert to a less crowded occupancy of the interior by the ribbons.

It follows from the resonance character of the Raman spectra that excitation by different laser lines detects the presence of different types of both nanotubes and nanoribbons. First, we determine the possible combinations starting from the diameter distribution of the applied P2-SWCNTs:[28] 1.4 nm average, containing 1.2−1.6 nm tubes,[29] then we select the ribbons that fit into the given cavities. We follow the numbering scheme for nanoribbons presented by Fujita[30] using the number of dimers (N) in the unit cell: the atomic width indicates the number of dimer lines in AGNRs and the number of zigzag lines in ZGNRs. Based on the observed RBM bands (Figure S1, Supporting Information), the three exciting lasers select the tubes in the 1.5−1.6 nm diameter range. We have calculated the width of the nanoribbons (solely the carbon network) by simply taking the distance between the outermost carbon atoms at the same position along the ribbon. The distances were calculated based on simple geometrical considerations giving negligible difference compared to the relaxed geometry published by Gillen et al.[31] (Note the slightly different definition of width for ZGNR.) The width was further increased by the projection of C−H bonds in the direction of the width. For the determination of the inner diameter of the smallest possible host carbon nanotubes, the carbon−hydrogen van der Waals distance was added to the width. These considerations lead to the possible nanoribbon types 4−7 AGNR and 3−4 ZGNR (see Figure S7 and Table S1, Supporting Information).

The RBLM of the 6-AGNR is clearly detected both with 633 and 532 nm excitation (Figure 2a,d). Its position is at 457 cm^{-1} with 633 nm excitation, which is slightly red-shifted compared to that of 6-AGNR@SWCNT prepared from the ferrocene precursor.[11] Theoretical estimates for this mode are 457,[11,32] 465.7,[27] and ∼453[33] cm^{-1}. Using 532 nm excitation, the RBLM is centered at 446 cm^{-1}. Since some nanotubes used in our experiment would also be of suitable size for the growth of either 5-AGNRs or 7-AGNRs, we searched for their signatures. We could observe neither the RBLM of the 7-AGNR at 397 cm^{-1} with the 532 nm laser[14] nor that of the 5-AGNR at 534 cm^{-1} with the 785 nm laser.[34] Thus, we can positively identify only the 6-AGNR, in accordance with TERS spectra (see below). As there are no experimental data for ZGNRs, we did not consider these conformations. As shown in Figure 2, the 6-AGNR modes are more intense in the 500 °C annealed sample using 532 nm excitation, while using 633 nm excitation the 600 °C annealed sample has stronger GNR signals (Figure 3). We presume this is caused by the presence of shorter ribbons at 500 °C, which results in a blueshift of their band gap.[35]

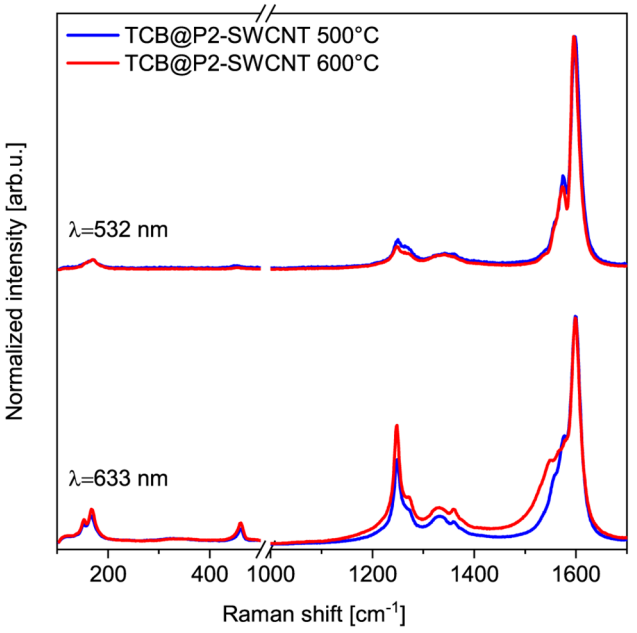

Figure 3. GNR@P2-SWCNT formed at 500 and 600 °C measured with 532 and 633 nm laser excitation. GNR intensity ratio of the 500 and 600 °C annealed sample changes with the excitation wavelength, indicating the presence of mostly shorter ribbons in the sample annealed at a lower temperature.

Since we do not know the reaction mechanism of the ribbon formation, there is no a priori knowledge of the range of the nanoribbons formed. Our case is more similar to the case of ferrocene, where the products could adapt to the diameter of the host tubes,[12] than to that of larger polyaromatic molecules where the type of nanoribbon is prepatterned by the precursors.[14,34] Most probably, our samples show a heterogeneity in diameter, ribbon type, and edge termination. C−Cl bending vibrations, found around 200 cm^{-1} in a TCB isomer,[36] are not detected in the Raman spectra. Energy-dispersive X-ray (EDX) spectra (Figure S5, Supporting Information), on the other hand, confirm the presence of Cl in the ribbons, indicating some chlorine termination, but quantitative information cannot be extracted. When estimating the possible fits of ribbon width and nanotube diameter, we have to allow for these ambiguities and also have to take into account that the hybrid structures are not exclusively the best tight fits.[14] The nanotube RBM signals can therefore originate from a subset of filled nanotubes within a certain diameter distribution as well as from empty nanotubes that fulfill the resonance condition. For this reason, we did not attempt to estimate a filling ratio or conversion yield from Raman spectra or compare it to other data in the literature.

The products formed inside the carbon nanotubes can be visualized using transmission electron microscopy. The encapsulated nanoribbons are sensitive to the electron beam; they twist upon illumination, which can help identify these

https://doi.org/10.1021/acs.jpclett.2c02046
J. Phys. Chem. Lett. 2022, 13, 9752−9758

structures.[7,16] Such twisting ribbons can be observed both in the 500 and 600 °C annealed samples (Figure 4). Confirming

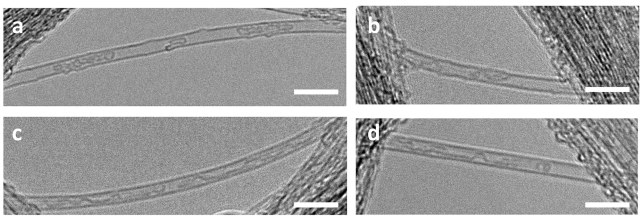

Figure 4. TEM images of the samples containing graphene nanoribbons formed at (a, b) 500 °C and (c, d) 600 °C. The scale bar on the images is 10 nm.

our spectroscopic observations, shorter (~20 nm) ribbons were observed in the sample annealed at 500 °C than in the 600 °C annealed one (>100 nm). TEM time sequences are shown in Figure S4, Supporting Information.

To further verify that the spectral signatures observed in the far-field measurements presented in Figures 2 and 3 arise from encapsulated ribbons as identified by TEM in Figure 4, we perform nanoscale imaging and spectroscopy using TERS. In Figure 5, we plot several images of a small nanotube bundle

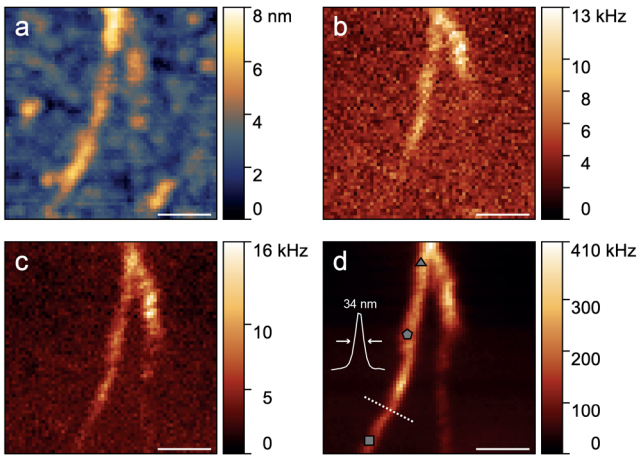

Figure 5. TERS of GNR@P2-SWCNT formed at 600 °C. (a) Topographic image acquired simultaneously with the optical information. (b–d) Optical image of the Stokes photons scattered by (b) the nanotube RBM, (c) the nanoribbon RBLM, and (d) the G mode of both nanotube and nanoribbon. The intensity profile in (d) extracted along the white dotted line indicates a spatial resolution of 34 nm. TERS spectra recorded at the marked locations are shown in Figure S6, Supporting Information. The length of the scale bars corresponds to 200 nm.

depicting topographical [Figure 5a] and optical [Figure 5b–d] information. The optical images in Figure 5b–d display the counts of Raman-scattered Stokes photons associated with the nanotube RBM, the ribbon RBLM, and the G mode from both nanotube and ribbon, respectively. Comparing these optical images clearly shows that the Raman signals arising from ribbon and nanotube are largely overlapping, indicating that ribbon formation occurs throughout the nanotubes and thus confirms the expected high filling ratio. TERS spectra recorded at the locations marked in Figure 5d are shown in Figure S6, Supporting Information, along with the corresponding far-field measurements.

In conclusion, we report a method for growing graphene nanoribbons inside carbon nanotubes from 1,2,4-trichlorobenzene, a liquid at room temperature. 6-AGNRs were identified and characterized by Raman spectroscopy, TERS, and TEM. The characteristic RBLM and C–H ipb modes of 6-AGNR were detected by far-field Raman spectroscopy and TERS. Following the Raman intensity of the C–H ipb peak it was possible to determine the ideal temperature for ribbon formation and, within that window, to follow the increase in length with increasing formation temperature. As the encapsulation step involves lower temperature than sublimation-based methods and no additional solvent, it results in fewer potential byproducts and higher purity.

EXPERIMENTAL METHODS

The precleaned nanotubes were opened, degassed, and immersed in 1,2,4-trichlorobenzene. The excess precursor was removed by filtration followed by evaporation of the solvent at room temperature.

Encapsulating 1,2,4-Trichlorobenzene into Carbon Nanotubes. P2-SWCNTs with 1.2–1.6 nm diameter range were purchased from Carbon Solutions, Inc.[28] TCB was purchased from Sigma-Aldrich. Before they were filled, P2-SWCNTs were placed in a quartz tube and heated at 420 °C for 20 min in air to open the ends of the tubes. After the nanotube caps were removed, functional groups that may block the open tube ends were removed by vacuum annealing. The tubes were placed under dynamic vacuum and inserted into a preheated furnace at 800 °C for 1 h, then cooled down to ambient temperate in steps of 5 °C/min. When the cleaned nanotubes reached room temperature, TCB was introduced into the quartz tube through a valve, without the nanotubes being exposed to air. The mixture (TCB@P2-SWCNT) was sonicated for 10 min and filtered after 24 h. To remove the molecules adsorbed on the walls, the TCB@P2-SWCNT was left open to air for 4 d.

Preparation of GNR@P2-SWCNT. To determine the ideal temperature for ribbon formation, TCB@P2-SWCNT samples were annealed from 100 to 1100 °C at 100 °C increments in a closed quartz tube. The annealing time at each temperature was kept for 12 h; the heating and cooling rate was 5 °C/min. After each annealing step the sample was analyzed using Raman spectroscopy through the quartz tube wall. Once the ideal ribbon formation temperature was determined (Figure 1), another portion of the filled sample was annealed directly to 500 °C and from there to 600 °C. During the direct annealing, when the cooling down started, one end of the quartz tube was kept at a lower temperature, to allow condensation of desorbed guest species and reaction products, if any.

Raman Characterization. This was carried out with a Renishaw InVia micro Raman spectrometer equipped with 532, 633, and 785 nm lasers. The measurements shown in Figure 1 were done using a sealed quartz ampule. The samples were kept in the ampule throughout the annealing sequence to prevent contamination. The micro-Raman specra were obtained through the quartz using 20× magnification objectives. Regular measurements were performed in air with a 100× magnification objective. Laser power was kept low to prevent heating-induced shift of the Raman peaks and sample damage.

Tip-Enhanced Raman Scattering. Samples for TERS were prepared by bath sonication in toluene (1 h at 45 kHz and 100 W followed by 30 min at 45 kHz and 30 W). While still

https://doi.org/10.1021/acs.jpclett.2c02046
J. Phys. Chem. Lett. 2022, 13, 9752–9758

sonicating, a drop of the solution was pipetted onto the surface of distilled water and transferred to a glass coverslip with gold markers for TERS measurements.

TERS measurements are performed using the setup described in ref 37. It consists of a home-built scanning probe microscope designed for noncontact shear-force operation with quartz tuning forks, on top of an inverted confocal microscope equipped with an x, y scan stage. A radially polarized HeNe laser beam (λ = 633 nm) is strongly focused by a high-numerical-aperture (NA 1.4) oil-immersion objective through the thin glass coverslip carrying the sample. The TERS probe, a gold micropyramid attached to the end of a quartz tuning fork, is positioned into the center of the laser focus, thus generating a nanoscale excitation source for Raman scattering. The distance between the sample surface and the TERS probe is controlled by means of a shear-force feedback system. The backscattered light is collected by the same objective used for excitation and filtered by a long-pass filter (LP633) to remove the Rayleigh component. For imaging, the sample is raster-scanned while the tip−sample distance is held constant and the Raman-scattered light is collected by an avalanche photodiode (APD). The spectral region of interest is selected by appropriate optical filters placed in front of the APD. For the RBM [Figure 5b], a band-pass filter centered at 632 nm and with a full width at half-maximum of 22 nm (BP632/22) is used; the RBLM [Figure 5c] is selected by a combination of LP647 and BP645/30; and for imaging of the G mode [Figure 5d], we employ a BP632/22 filter. Full spectra (see Figure S6) are recorded using a CCD-equipped spectrometer. More details about the experimental implementation and the principles of TERS can be found in ref 37.

High-Resolution Transmission Electron Microscopy. High-resolution TEM imaging was performed using a JEOL 2100F TEM (field emission gun source, information limit less than 0.19 nm) at 100 kV at room temperature. EDX spectra were recorded using an Oxford Instruments 30 mm^2 Si(Li) detector or an Oxford Instruments x-Max 80 SDD running on an INCA microanalysis system. Samples for TEM and EDX were prepared by casting several drops of a suspension of nanotubes onto copper-grid mounted "lacey" carbon films.

■ ASSOCIATED CONTENT

Supporting Information

The Supporting Information is available free of charge at https://pubs.acs.org/doi/10.1021/acs.jpclett.2c02046.

Additional Raman spectra, TEM time sequences, TERS spectra, AGNR width estimations (PDF)

Transparent Peer Review report available (PDF)

■ AUTHOR INFORMATION

Corresponding Authors

Ana Cadena − *Institute for Solid State Physics and Optics, Wigner Research Centre for Physics, 1525 Budapest, Hungary; Department of Chemical and Environmental Process Engineering, Faculty of Chemical Technology and Biotechnology, Budapest University of Technology and Economics, 1111 Budapest, Hungary*; Email: anacristina.cadena@wigner.hu

Bea Botka − *Institute for Solid State Physics and Optics, Wigner Research Centre for Physics, 1525 Budapest, Hungary*; orcid.org/0000-0003-3707-3097; Email: botka.bea@wigner.hu

Authors

Áron Pekker − *Institute for Solid State Physics and Optics, Wigner Research Centre for Physics, 1525 Budapest, Hungary*; orcid.org/0000-0003-1075-0502

Cla Duri Tschannen − *Photonics Laboratory, ETH Zürich, 8093 Zürich, Switzerland*

Chiara Lombardo − *Photonics Laboratory, ETH Zürich, 8093 Zürich, Switzerland*

Lukas Novotny − *Photonics Laboratory, ETH Zürich, 8093 Zürich, Switzerland*; orcid.org/0000-0002-9970-8345

Andrei N. Khlobystov − *Department of Chemistry, University of Nottingham, NG7 2RD Nottingham, United Kingdom*; orcid.org/0000-0001-7738-4098

Katalin Kamarás − *Institute for Solid State Physics and Optics, Wigner Research Centre for Physics, 1525 Budapest, Hungary*; orcid.org/0000-0002-0390-3331

Complete contact information is available at: https://pubs.acs.org/10.1021/acs.jpclett.2c02046

Notes

The authors declare no competing financial interest.

■ ACKNOWLEDGMENTS

We thank S. Pekker and D. Földes for enlightening discussions. Funding for this research was provided by the Hungarian National Research, Development and Innovation Office under Grant Nos. FK 125063 and FK 138411 and by the Swiss National Science Foundation under Grant No. 200020_192362/1. Research infrastructure in Hungary was provided by the Hungarian Academy of Sciences. The authors thank the Nanoscale & Microscale Research Centre (nmRC), University of Nottingham, for enabling access to HRTEM instrumentation.

■ REFERENCES

(1) Wang, X.-Y.; Narita, A.; Müllen, K. Precision synthesis versus bulk-scale fabrication of graphenes. *Nat. Rev. Chem.* **2018**, *2*, 0100−1−10.

(2) Tapasztó, L.; Dobrik, G.; Lambin, P.; Biró, L. P. Tailoring the atomic structure of graphene nanoribbons by scanning tunneling microscope litography. *Nat. Nanotechnol.* **2008**, *3*, 397−401.

(3) Wu, J.; Gherghel, L.; Watson, M. D.; Li, J.; Wang, Z.; Simpson, C. D.; Kolb, U.; Müllen, K. From branched polyphenylenes to graphite ribbons. *Macromolecules* **2003**, *36*, 7082−7089.

(4) Yang, X.; Dou, X.; Rouhanipour, A.; Zhi, L.; Räder, J.; Müllen, K. Two-dimensional graphene nanoribbons. *J. Am. Chem. Soc.* **2008**, *130*, 4216−4217.

(5) Cai, J.; Ruffieux, P.; Jaafar, R.; Bieri, M.; Braun, T.; Blankenburg, S.; Muoth, M.; Seitsonen, A.; Saleh, M.; Feng, X.; Müllen, K.; Fasel, R. Atomically precise bottom-up fabrication of graphene nanoribbons. *Nature* **2010**, *466*, 470−473.

(6) Houtsma, R.; de la Rie, J.; Stöhr, M. Atomically precise graphene nanoribbons: interplay of structural and electronic properties. *Chem. Soc. Rev.* **2021**, *50*, 6541−6568.

(7) Lim, H. E.; Miyata, Y.; Kitaura, R.; Nishimura, Y.; Nishimoto, Y.; Irle, S.; Warner, J. H.; Kataura, H.; Shinohara, H. Growth of carbon nanotubes via twisted graphene nanoribbons. *Nat. Commun.* **2013**, *4*, 2548−1−7.

(8) Fujihara, M.; Miyata, Y.; Kitaura, R.; Nishimura, O.; Camacho, C.; Irle, S.; Iizumi, Y.; Okazaki, T.; Shinohara, H. Dimerization-initiated preferential formation of coronene-based graphene nanoribbons in carbon nanotubes. *J. Phys. Chem. C* **2012**, *116*, 15141−15145.

(9) Botka, B.; Füstös, M. E.; Tóháti, H. M.; Németh, K.; Klupp, G.; Szekrényes, Z.; Kocsis, D.; Utczás, M.; Székely, E.; Váczi, T.; Tarczay, G.; Hackl, R.; Chamberlain, T. W.; Khlobystov, A. N.; Kamarás, K.

Interactions and chemical transformations of coronene inside and outside carbon nanotubes. *Small* **2014**, *10*, 1369−1378.
(10) Talyzin, A. V.; Anoshkin, I. V.; Krasheninnikov, A. V.; Nieminen, R. M.; Nasibulin, A. G.; Jiang, H.; Kauppinen, E. I. Synthesis of graphene nanoribbons encapsulated in single-walled carbon nanotubes. *Nano Lett.* **2011**, *11*, 4352−4356.
(11) Kuzmany, H.; Shi, L.; Martinati, M.; Cambré, S.; Wenseleers, W.; Kürti, J.; Koltai, J.; Kukucska, G.; Cao, K.; Kaiser, U.; Saito, T.; Pichler, T. Well-defined sub-nanometer graphene ribbons synthesized inside carbon nanotubes. *Carbon* **2021**, *171*, 221−229.
(12) Zhang, Y.; Cao, K.; Saito, T.; Kataura, H.; Kuzmany, H.; Pichler, T.; Kaiser, U.; Yang, G.; Shi, L. Carbon nanotube-dependent synthesis of armchair graphene nanoribbons. *Nano Res.* **2022**, *15*, 1709−1714.
(13) Chamberlain, T. W.; et al. Stop-frame filming and discovery of reactions at the single-molecule level by transmission electron microscopy. *ACS Nano* **2017**, *11*, 2509−2520.
(14) Kinno, Y.; Omachi, H.; Shinohara, H. Template synthesis of armchair-edge graphene nanoribbons inside carbon nanotubes. *Appl. Phys. Express* **2020**, *13*, 015002−1−4.
(15) Chuvilin, A.; Bichoutskaia, E.; Gimenez-Lopez, M. C.; Chamberlain, T. W.; Rance, G. A.; Kuganathan, N.; Biskupek, J.; Kaiser, U.; Khlobystov, A. N. Self-assembly of a sulphur-terminated graphene nanoribbon within a single-walled carbon nanotube. *Nat. Mater.* **2011**, *10*, 687−692.
(16) Chamberlain, T. W.; Biskupek, J.; Rance, G. A.; Chuvilin, A.; Alexander, T. J.; Bichoutskaia, E.; Kaiser, U.; Khlobystov, A. N. Size, structure, and helical twist of graphene nanoribbons controlled by confinement in carbon nanotubes. *ACS Nano* **2012**, *6*, 3943−3953.
(17) Cadena, A.; Botka, B.; Kamarás, K. Organic molecules encapsulated in single-walled carbon nanotubes. *Oxford Open Materials Science* **2020**, *1*, itab009−1−16.
(18) Yudasaka, M.; Ajima, K.; Suenaga, K.; Ichihashi, T.; Hashimoto, A.; Iijima, S. Nano-extraction and nano-condensation for C_{60} incorporation into single-wall carbon nanotubes in liquid phases. *Chem. Phys. Lett.* **2003**, *380*, 42−46.
(19) Miners, S. A.; Rance, G. A.; Khlobystov, A. N. Chemical reactions confined within carbon nanotubes. *Chem. Soc. Rev.* **2016**, *45*, 4727−4746.
(20) Campo, J.; Piao, Y.; Lam, S.; Stafford, C.; Streit, J.; Simpson, J.; Hight Walker, A.; Fagan, J. Enhancing single-Wall carbon nanotube properties through controlled endohedral filling. *Nanoscale Horiz* **2016**, *1*, 317−324.
(21) Campo, J.; Cambré, S.; Botka, B.; Obrzut, J.; Wenseleers, W.; Fagan, J. Optical property tuning of single-wall carbon nanotubes by endohedral encapsulation of a wide variety of dielectric molecules. *ACS Nano* **2021**, *15*, 2301−2317.
(22) Dresselhaus, M.; Jorio, A.; Hofmann, M.; Dresselhaus, G.; Saito, R. Perspectives on carbon nanotubes and graphene Raman spectroscopy. *Nano Lett.* **2010**, *10*, 751−758.
(23) Almadori, Y.; Alvarez, L.; Le Parc, R.; Aznar, R.; Fossard, F.; Loiseau, A.; Jousselme, B.; Campidelli, S.; Hermet, P.; Belhboub, A.; Rahmani, A.; Saito, T.; Bantignies, J.-L. Chromophore ordering by confinement into carbon nanotubes. *J. Phys. Chem. C* **2014**, *118*, 19462−19468.
(24) Wenseleers, W.; Cambré, S.; Čulin, J.; Bouwen, A.; Goovaerts, E. Effect of water filling on the electronic and vibrational resonances of carbon nanotubes: Characterizing tube opening by Raman spectroscopy. *Adv. Mater.* **2007**, *19*, 2274−2278.
(25) Longhurst, M. J.; Quirke, N. The environmental effect on the radial breathing mode of carbon nanotubes. II. Shell model approximation for internally and externally adsorbed fluids. *J. Chem. Phys.* **2006**, *125*, 184705−1−6.
(26) Cambré, S.; Schoeters, B.; Luyckx, S.; Goovaerts, E.; Wenseleers, W. Experimental observation of single-file water filling of thin single-wall carbon nanotubes down to chiral index (5,3). *Phys. Rev. Lett.* **2010**, *104*, 207401−1−4.
(27) Zhou, J.; Dong, J. Vibrational property and Raman spectrum of carbon nanoribbon. *Appl. Phys. Lett.* **2007**, *91*, 173108−1−3.
(28) Carbon Solutions, Inc. Online at http://www.carbonsolution.com, Accessed: 2022-08-15.
(29) Pekker, Á.; Kamarás, K. Wide-range optical studies on various single-walled carbon nanotubes: origin of the low-energy gap. *Phys. Rev. B* **2011**, *84*, 075475.
(30) Fujita, M.; Wakabayashi, K.; Nakada, K.; Kusakabe, K. Peculiar localized state at zigzag graphite edge. *J. Phys. Soc. Jpn.* **1996**, *65*, 1920−1923.
(31) Gillen, R.; Mohr, M.; Thomsen, C.; Maultzsch, J. Vibrational properties of graphene nanoribbons by first-principles calculations. *Phys. Rev. B* **2009**, *80*, 155418.
(32) Ma, C.; Liang, L.; Xiao, Z.; Puretzky, A. A.; Hong, K.; Lu, W.; Meunier, V.; Bernholc, J.; Li, A.-P. Seamless staircase electrical contact to semiconducting graphene nanoribbons. *Nano Lett.* **2017**, *17*, 6241−6247.
(33) Liu, D.; Daniels, C.; Meunier, V.; Every, A. G.; Tománek, D. In-plane breathing and shear modes in low-dimensional nanostructures. *Carbon* **2020**, *157*, 364−370.
(34) Milotti, V.; Berkmann, C.; Laranjeira, J.; Cui, W.; Cao, K.; Zhang, Y.; Kaiser, U.; Yanagi, K.; Melle-Franco, M.; Shi, L.; Pichler, T.; Ayala, P. Unravelling the complete Raman response of graphene nanoribbons discerning the signature of edge passivation. *Small Methods* **2022**, *6*, 2200110−1−8.
(35) Talirz, L.; Söde, H.; Kawai, S.; Ruffieux, P.; Meyer, E.; Feng, X.; Müllen, K.; Fasel, R.; Pignedoli, C. A.; Passerone, D. Band gap of atomically precise graphene nanoribbons as a function of ribbon length and termination. *ChemPhysChem* **2019**, *20*, 2348−2353.
(36) Saëki, S. The Raman spectra of 1,3,5-trichlorobenzene and 1,3,5-trichlorobenzene-d_3. *Bull. Chem. Soc. Jpn.* **1961**, *34*, 1851−1858.
(37) Tschannen, C. D.; Vasconcelos, T. L.; Novotny, L. Tip-enhanced Raman spectroscopy of confined carbon chains. *J. Chem. Phys.* **2022**, *156*, 044203.

https://doi.org/10.1021/acs.jpclett.2c02046
J. Phys. Chem. Lett. 2022, 13, 9752−9758